

A Severe Acute Respiratory Syndrome Coronavirus That Lacks the E Gene Is Attenuated In Vitro and In Vivo[∇]

Marta L. DeDiego,¹ Enrique Álvarez,¹ Fernando Almazán,¹ María Teresa Rejas,² Elaine Lamirande,³ Anjeanette Roberts,³ Wun-Ju Shieh,⁴ Sherif R. Zaki,⁴ Kanta Subbarao,³ and Luis Enjuanes^{1*}

Department of Molecular and Cell Biology, Centro Nacional de Biotecnología (CSIC), Campus Universidad Autónoma, Darwin 3, Cantoblanco, 28049 Madrid, Spain¹; Centro de Biología Molecular (CSIC-UAM), Facultad de Ciencias, Campus Universidad Autónoma, Cantoblanco, 28049 Madrid, Spain²; Laboratory of Infectious Diseases, National Institute of Allergy and Infectious Diseases, National Institutes of Health, Bethesda, Maryland 20892³; and Infectious Disease Pathology Activity, National Center for Infectious Diseases, Centers for Disease Control and Prevention, Atlanta, Georgia 30333⁴

Received 11 July 2006/Accepted 8 November 2006

A deletion mutant of severe acute respiratory syndrome coronavirus (SARS-CoV) has been engineered by deleting the structural E gene in an infectious cDNA clone that was constructed as a bacterial artificial chromosome (BAC). The recombinant virus lacking the E gene (rSARS-CoV-ΔE) was rescued in Vero E6 cells. The recovered deletion mutant grew in Vero E6, Huh-7, and CaCo-2 cells to titers 20-, 200-, and 200-fold lower than the recombinant wild-type virus, respectively, indicating that although the E protein has an effect on growth, it is not essential for virus replication. No differences in virion stability under a wide range of pH and temperature were detected between the deletion mutant and recombinant wild-type viruses. Although both viruses showed the same morphology by electron microscopy, the process of morphogenesis seemed to be less efficient with the defective virus than with the recombinant wild-type one. The rSARS-CoV-ΔE virus replicated to titers 100- to 1,000-fold lower than the recombinant wild-type virus in the upper and lower respiratory tract of hamsters, and the lower viral load was accompanied by less inflammation in the lungs of hamsters infected with rSARS-CoV-ΔE virus than with the recombinant wild-type virus. Therefore, the SARS-CoV that lacks the E gene is attenuated in hamsters, might be a safer research tool, and may be a good candidate for the development of a live attenuated SARS-CoV vaccine.

Severe acute respiratory syndrome (SARS) is a respiratory disease characterized by an atypical pneumonia, caused by a novel coronavirus (CoV) (13, 15, 27, 28, 35, 41, 45). The disease was reported for the first time in Guangdong Province, China, at the end of 2002, and spread to 32 countries in the course of a few months. After July 2003, only 4 community-acquired SARS cases were reported in China, but there have been at least as many reports of laboratory-acquired infections, with secondary spread in one case. Efficacious therapy is not available for this life-threatening disease that caused a mortality of about 10% in the epidemic of 2002 to 2003. Therefore, it is of interest to engineer attenuated SARS-CoVs as safer research tools.

SARS-CoV is an enveloped virus of the *Coronaviridae* family, group 2, and has a single-stranded, positive-sense 29.7-kb RNA genome (18, 48). Coronaviruses replicate in the cell cytoplasm and encode a nested set of mRNA molecules of different sizes. Viral genome expression begins with the translation of two large polyproteins, pp1a and pp1ab, including the viral replicase genes (50). Expression of the open reading frame (ORF) 1ab involves a ribosomal frameshifting into the –1 frame just upstream of the ORF 1a translation termination codon (4). The pp1a and pp1ab polyproteins are processed by

viral proteinases to yield functional components of the membrane-bound replicase complex (59). The replicase complex is involved in genome replication and transcription of subgenomic mRNAs (sgmRNAs), encoding structural proteins, such as the spike (S), envelope (E), membrane (M), and nucleocapsid (N), and a set of nonstructural proteins, whose sequence and number differ between the different species of coronavirus (47). In the case of SARS-CoV, ORFs 3a and 7a encode additional structural proteins (22, 25, 46). Among human CoVs (HCoVs), such as HCoV-229E, HCoV-OC43, SARS-CoV, HCoV-NL63, and Hong Kong University 1-CoV, SARS-CoV causes the most severe disease (52, 54).

The virion envelope of CoVs contains at least three structural proteins, S, E, and M, embedded in the membrane. SARS-CoV has an additional structural membrane protein, 3a (25, 46). CoV M and E proteins are key factors for virus assembly and budding (6–8, 11, 14, 30). In fact, expression of these proteins in cell lines results in the production of virus-like particles (VLPs) (3, 8, 23, 53). In the case of SARS-CoV, there are conflicting reports on the proteins necessary for the formation of VLPs. Some reports describe the requirement of E and M for the efficient assembly of pseudoparticles in insect cells (21, 36), whereas others suggest that E protein is not essential for SARS-CoV-like particle formation in mammalian cells and propose that M and N proteins play a major role in morphogenesis (23).

The CoV E protein is present in virions in low copy number as a transmembrane protein (30, 34, 42). E protein contains a short (7 to 9 amino acid) hydrophilic amino terminus region and a 21- to 29-amino-acid hydrophobic region, followed by a

* Corresponding author. Mailing address: Department of Molecular and Cell Biology, Centro Nacional de Biotecnología, CSIC, Darwin 3, Campus Universidad Autónoma, Cantoblanco, 28049 Madrid, Spain. Phone: 34 91 585 4555. Fax: 34 91 585 4915. E-mail: L.Enjuanes@cnb.uam.es.

[∇] Published ahead of print on 15 November 2006.

hydrophilic carboxy terminus (6, 7). The SARS-CoV E protein contains an unusually short, palindromic transmembrane helical hairpin predicted around a previously unidentified pseudo-center of symmetry (2, 26). This hairpin possibly modifies lipid bilayers by increasing their curvature and likely plays a pivotal role in viral budding.

CoV E proteins share several characteristics with proteins of other viruses that function as ion channels, having a highly hydrophobic domain that forms at least one amphipathic α -helix that oligomerizes to form a putative ion-conductive pore in membranes (51). SARS-CoV and murine hepatitis virus (MHV) E proteins alter membrane permeability (31–33). Furthermore, HCoV-229E, MHV, SARS-CoV, and infectious bronchitis virus (IBV) E proteins form ion channels that are more permeable to monovalent cations than to monovalent anions (55, 56). The transmissible gastroenteritis virus (TGEV) E protein is essential for the production of recombinant infectious virus (9, 39). In contrast, MHV E protein is critical but not essential for virus replication because an MHV mutant in which the E gene has been deleted grows in cell culture to titers that are at least 3 orders of magnitude lower than recombinant wild-type viruses (30).

In this article, we report the generation of a recombinant SARS-CoV (rSARS-CoV) mutant in which expression of the E gene was abolished in a SARS-CoV cDNA clone that was assembled as a bacterial artificial chromosome (BAC). Although maximal virus titers reached by this defective virus were lower than those of the recombinant wild-type virus, the Δ E virus infected different cell lines, indicating that E protein is important but not essential for SARS-CoV replication. This rSARS-CoV- Δ E virus was attenuated in vivo, making it a safer research tool and a promising vaccine candidate.

MATERIALS AND METHODS

Virus. An infectious cDNA clone of the Urbani strain of SARS-CoV has been constructed in our laboratory and assembled as a BAC (1). SARS-CoV RNA was kindly provided by the Centers for Disease Control and Prevention, Atlanta, GA. All work with infectious viruses and infected animals was performed in biosafety level 3 facilities by personnel wearing positive-pressure air-purifying respirators (HEPA AirMate; 3M, Saint Paul, MN).

Cells. The African green monkey kidney-derived Vero E6 cells were kindly provided by Eric Snijder (Medical Center, University of Leiden, The Netherlands). The human colon carcinoma-derived CaCo-2 cells were obtained from the European Collection of Cell Cultures. The human liver-derived Huh-7 cells were kindly provided by R. Bartenschlager (Department of Molecular Virology, University of Heidelberg, Germany) (16, 20, 37). In all cases, cells were grown in Dulbecco's modified Eagle's medium (GIBCO) supplemented with 25 mM HEPES and 10% fetal bovine serum (Biowhittaker). Virus titrations were performed in Vero E6 or Vero cells following standard procedures using closed flasks or plates sealed in plastic bags. For plaque assays, cells were fixed with 10% formaldehyde and stained with crystal violet 2 days postinfection. For 50% tissue culture infectious dose (TCID₅₀) assays, cytopathic effect was recorded 4 days postinfection.

Construction of plasmid pBAC-SARS-CoV- Δ E. The pBAC-SARS-CoV- Δ E plasmid encoding a rSARS-CoV lacking the E gene was constructed from a previously generated full-length infectious cDNA clone (plasmid pBAC-SARS-CoV^{FL}) (1). The E gene deletion was introduced by overlap extension PCR using the plasmid pBAC-SARS-CoV^{FL}. The oligonucleotides SARS-E-VS (5'-CTCTTCAGGATTGCTAATCCAGCAATGG-3') and SARS-26326- Δ E-RS (5'-CTCCAGAAGAGTTTCAGATTTTTAAACACGCTTAACGTACCTGTTTCTCCGSAACGAGATTGACTACACAAATGGTACTCACTTCTTGCTGTACTAC-3'), which includes a deletion between nucleotides (nt) 26155 and 26296 of the SARS-CoV genome, two point mutations in the core sequence (CS) of E gene transcription-regulating sequence (TRS), and one point mutation, which abrogates the start ATG codon of this gene, were used to generate a

PCR product from nt 26018 to 26326 of the SARS-CoV genome. The oligonucleotides SARS-26297-VS (5'-GCGTGTAAAAAATCTGAACTCTTCTGAA GG-3') and SARS-N733-RS (5'-GGCCTGTGTGTGTGGCC-3') were used to generate a PCR product spanning nt 26297 to 28853 of the SARS-CoV genome. Both overlapping products were used as templates for PCR amplification using primers SARS-E-VS and SARS-N733-RS. The final PCR product was digested with the enzymes BamHI and NheI and cloned into the intermediate plasmid pBAC-SARS-5'-3'-DN to generate the plasmid pBAC-SARS-5'-3'-DN- Δ E. Plasmid pBAC-SARS-5'-3'-DN contains the first 7,452 nt of the SARS-CoV genome under the cytomegalovirus promoter and the last 3,683 nt followed by a 25-bp synthetic poly(A), the hepatitis delta virus ribozyme, and the bovine growth hormone termination and polyadenylation sequences to make an accurate 3' end. Finally, the BamHI-RsrII fragment of pBAC-SARS-CoV^{FL} plasmid, corresponding to nt 26045 to 29783, was exchanged with that of plasmid pBAC-SARS-5'-3'-DN- Δ E to generate the plasmid pBAC-SARS-CoV- Δ E.

Transfection and recovery of infectious viruses from the cDNA clones. Vero E6 cells grown to 90% confluence in 12.5-cm² flasks were transfected with 6 μ g of the plasmid pBAC-SARS-CoV- Δ E or pBAC-SARS-CoV^{FL} as a control, using 12 μ g of Lipofectamine 2000 (Invitrogen) according to manufacturer's instructions. After an incubation period of 6 h at 37°C, the transfection media were replaced and cells were incubated at 37°C for 72 h. Cell supernatants were harvested and passaged twice on fresh Vero E6 cells, and the recovered viruses were cloned by three rounds of plaque purification.

rSARS-CoV- Δ E growth kinetics. Subconfluent monolayers (90% confluence) of Vero E6, Huh-7, and CaCo-2 cells were infected at a multiplicity of infection (MOI) of 0.5 with the viruses rSARS-CoV- Δ E and rSARS-CoV. Culture supernatants were collected at different times postinfection, and virus titers were determined as described above.

RNA analysis by RT-PCR. Total RNA from Vero E6-infected cells was extracted using the QIAGEN RNeasy kit according to the manufacturer's instructions and used for reverse transcription (RT)-PCR analysis of S, E, and N gene mRNA transcription. Reactions were performed at 42°C for 1 h using Moloney leukemia virus reverse transcriptase (Ambion) and the antisense primers SARS-S613-RS (5'-CATCTATAGTTGATAGCCC-3'), complementary to nt 594 to 613 of S gene; SARS-E231-RS (5'-TTAGACCAGAAGATCAGGAAGCTCC-3'), complementary to nt 208 to 231 of E gene; and URB-28630-RS (5'-TGCTTCCCTCTGCGTAGAAGCC-3'), complementary to nt 511 to 532 of N gene. The cDNAs were amplified by PCR using the virus sense primer URB-29-VS (5'-GCCAACCAACCTCGATCTCTTG-3'), spanning nucleotides 29 to 50 of the SARS-CoV leader sequence, and the reverse primers described for the RT reactions. The RT-PCR products were resolved by electrophoresis in 0.8% agarose gels.

Total RNA from rSARS-CoV- and rSARS-CoV- Δ E-infected Vero E6 cells was extracted at 7 h postinfection as described above. This RNA was used as a template for quantitative real-time RT-PCR analysis of sgRNA transcription. Reactions were performed at 50°C using the ThermoScript retrotranscriptase (Invitrogen) and the reverse primers indicated in Table 1. The cDNAs were amplified by PCR using the Power SYBR green PCR master mix (Applied Biosystems) and the oligonucleotides described in Table 1. For each mRNA, a primer hybridizing in the leader sequence and another primer hybridizing in each coding sequence were used. For the genomic RNA, primers hybridizing near the 5' end of the replicase were used. All of the primers were designed by using the Primer Express software (Applied Biosystems).

Western blotting. Cell lysates were analyzed by sodium dodecyl sulfate-polyacrylamide gel electrophoresis. Proteins were transferred to a nitrocellulose membrane with a Bio-Rad mini protein II electroblotting apparatus at 150 mA for 2 h in 25 mM Tris–192 mM glycine buffer, pH 8.3, containing 20% methanol. Membranes were blocked for 1 h with 5% dried skim milk in TBS (20 mM Tris-HCl, pH 7.5, 150 mM NaCl) and incubated with polyclonal antibodies specific for N, S (dilution 1:500; Imgenex), and E proteins (dilution 1:2,000; kindly provided by Shen Shuo, Institute of Molecular and Cellular Biology, Singapore). Bound antibody was detected with horseradish peroxidase-conjugated goat anti-rabbit antibody (Cappel) and the ECL detection system (Amersham Pharmacia Biotech).

Indirect immunofluorescence microscopy. Subconfluent Vero E6 cells grown in 9-cm² slide flasks were infected at an MOI of 1. At 24 h postinfection, cells were washed in ice-cold phosphate-buffered saline (PBS) and fixed with 8% paraformaldehyde for 30 min at room temperature. The cells were then permeabilized with 0.2% saponin in blocking solution (PBS, pH 7.4, containing 10% fetal bovine serum) for 1 h at room temperature and incubated with a polyclonal SARS-CoV specific antibody, kindly provided by Anlong Xu (Zhongshan University, Guangzhou, China) for 90 min at room temperature. Cells were then washed three times with PBS, incubated with Cy5-conjugated anti-human im-

TABLE 1. Primers used for checking the expression of viral sgmRNAs by quantitative RT-PCR

sgmRNA	Primer	Sequence (5'-3')	Length (nt)	PCR product size (bp)
1	Q-SARS-1931-VS	ACCACTCAATTCTTGATTGCA	22	85
	Q-SARS-2015-RS	ATGGCGTCGACAAGACGTAAT	21	
2	Q-SsgSARS-VS	CAACCTCGATCTCTGTAGATCTGTT	26	96
	Q-SsgSARS-RS	TGCACCGGTCAAGGTCACTA	20	
3	Q-3sgSARS-VS	TACCCAGGAAAAGCCAACCA	20	150
	Q-3sgSARS-RS	GCATGAACAGTACTTGCAGGAGA	23	
4	Q-NsgSARS-VS	AAGCCAACCAACCTCGATCTC	21	128
	Q-EsgSARS-RS	AAGAATACCACGAAAGCAAGAAAAA	25	
5	Q-NsgSARS-VS	AAGCCAACCAACCTCGATCTC	21	134
	Q-MsgSARS-RS	AGTTGTTAAGCTCCTCAACGGTAA	25	
6	Q-NsgSARS-VS	AAGCCAACCAACCTCGATCTC	21	75
	Q-6sgSARS-RS	GCGACGTCCTAATTTGTAATAAGA	25	
7	Q-NsgSARS-VS	AAGCCAACCAACCTCGATCTC	21	107
	Q-7sgSARS-RS	GATAGTGATATAGCTCGCAAGATGTAATAC	31	
8	Q-8sgSARS-VS	CAACCTCGATCTTGTAGATCTGTT	26	83
	Q-8sgSARS-RS	GCAACTGCATAGAGAAATACAAGTCAA	27	
9	Q-NsgSARS-VS	AAGCCAACCAACCTCGATCTC	21	118
	Q-NsgSARS-RS	TGGGTCCACCAAATGTAATGC	21	

munoglobulin G (Jackson ImmunoResearch) at a 1:200 dilution in blocking solution for 30 min at room temperature, and washed five times with PBS. The slides were removed, mounted with glass coverslips, and analyzed with a Zeiss Axiophot fluorescence microscope.

Electron microscopy. For conventional electron microscopy, Vero E6 cell monolayers were infected with rSARS-CoV and rSARS-CoV-ΔE viruses at an MOI of 1. The cells were fixed in situ 20 h postinfection with 2% glutaraldehyde in phosphate Na/K buffer (pH 7.4) for 1 h at room temperature. Cells were removed from the dishes in the fixative and transferred to Eppendorf tubes. After centrifugation, cells were washed three times in phosphate Na/K buffer (pH 7.4) and processed for embedding in epoxy TAAB 812 resin (TAAB Laboratories, Berkshire, England) according to standard procedures. Cells were treated with a mixture of 1% osmium tetroxide and 0.8% potassium ferricyanide in distilled water for 1 h at 4°C. After five washes with distilled water, samples were incubated with 2% uranyl acetate in water for 1 h, washed three times, and dehydrated twice in increasing concentrations of acetone (50, 70, 90, and 100%) for 10 min each at room temperature. Infiltration of resin was accomplished in increasing concentrations of acetone-Epon (3:1, 1:1, 1:3, and 100% Epon). Polymerization of infiltrated samples was done at 60°C for 2 days. Ultrathin sections of the samples were stained with saturated uranyl acetate and lead citrate and examined at 80 kV in a Jeol JEM-1010 (Tokyo, Japan) electron microscope.

For negative-staining electron microscopy, supernatants of Vero E6 cells infected for 20 h were fixed with 10% formaldehyde and concentrated onto carbon-coated ionized copper grids in a Beckman airfuge at 21 lb/in² using an electron microscopy rotor (EM-90; Beckman). Grids were stained with 2% phosphotungstic acid, pH 7, for 1 min. Samples were examined by electron microscopy as described above.

Virus replication in hamsters. The animal protocol employed in this study was approved by the National Institute of Allergy and Infectious Disease Animal Care and Use Committee. Male Golden Syrian hamsters, LVG (SYR), were obtained from Charles River Laboratories (Wilmington, MA) and pair-housed in individually ventilated microisolator rodent cages. Hamsters were rested for at least 3 days before initiation of the following experiments. Golden Syrian hamsters (44 days of age) were lightly anesthetized by isoflurane (USP-Baxter Healthcare, Deerfield, IL) inhalation and inoculated intranasally with 10³ TCID₅₀ of rSARS-CoV or rSARS-CoV-ΔE in a 100-μl total volume. Hamsters were sacrificed 2, 5, and 8 days after virus inoculation (4 hamsters/group/day), and lungs and nasal turbinates were harvested and stored frozen. For viral titer determination, tissue samples were thawed, weighed, and homogenized to a final 10% (wt/vol) suspension in Leibovitz's L-15 medium (Invitrogen, Grand Island, NY) with gentamicin (Invitrogen) and amphotericin B (Quality Biological, Gaithersburg, MD), which were added to the tissue culture medium at final concentrations of 0.1 mg/liter and 5 mg/liter, respectively. Tissue homogenates were clarified by low-speed centrifugation, and virus titers were determined in Vero cell monolayers in 24- and 96-well plates as described previously (49). Virus titers are expressed as TCID₅₀/g of tissue, with a lower limit of detection of 10^{1.5} TCID₅₀/g. It has been determined that 0.7 PFU is equivalent to 1 TCID₅₀.

Histopathologic examination of lungs from infected hamsters. Isoflurane-anesthetized Golden Syrian hamsters (40 days of age) were inoculated intranasally with 10³ TCID₅₀ rSARS-CoV (1 hamster/day) or rSARS-CoV-ΔE (2 hamsters/day) in a 100-μl total volume. Hamsters were sacrificed 2 and 5 days after infection; lungs were inflated with and fixed in 10% neutral buffered formalin for 3 days, routinely processed, and embedded in paraffin subsequently. Histopathologic examination was performed by using hematoxylin- and eosin-stained sections.

Immunohistochemistry. A colorimetric indirect immunalkaline phosphatase immunohistochemistry method was developed by using a mouse anti-SARS-CoV antibody (49). In brief, 3-μm sections from formalin-fixed, paraffin-embedded tissues were deparaffinized, rehydrated, and placed in a DAKO autostainer (DAKO Corporation, Carpinteria CA). The sections were digested in 0.1 mg/ml Proteinase K (Boehringer-Mannheim Corporation, Indianapolis, IN) and then incubated for 1 h with a hyperimmune mouse ascitic fluid reactive with SARS-CoV antigen at a 1:1,000 dilution. After incubation, slides were washed and incubated with a biotinylated anti-mouse antibody. Antigens were visualized by using a streptavidin-alkaline phosphatase complex followed by naphthol/fast red substrate for colorimetric detection (DAKO Corporation). Sections were counterstained with Mayer's hematoxylin (Fisher Scientific, Pittsburgh, PA).

RESULTS

Rescue of a rSARS-CoV mutant defective in the E gene. To study the requirement of the E gene in the viral cycle of SARS-CoV, a cDNA clone with the E gene deleted was constructed as a BAC. The expression of the E protein was abrogated by the introduction of point mutations within the TRS and at the start ATG codon of E gene (Fig. 1A) (50, 60). The introduced mutations were silent for gene 3b that partially overlaps with the E gene. In addition, to avoid the possibility of genetic reversion of the recombinant virus, a 142-nt segment covering the majority of the E gene was deleted. To maintain the wild-type transcription levels of the M gene, 48 nt upstream of the published TRS of this gene at the 3' end of the E gene were not altered (50). Vero E6 cells were transfected with plasmid pBAC-SARS-CoV-ΔE or with the parental plasmid pBAC-SARS-CoV^{FL}, and propagation-competent viruses (rSARS-CoV-ΔE and recombinant wild-type rSARS-CoV) were recovered from both plasmids with relatively high virus titers, even for the rSARS-CoV-ΔE virus (>10⁵ PFU/ml). The cytopathic effect characterized by the rounding and detach-

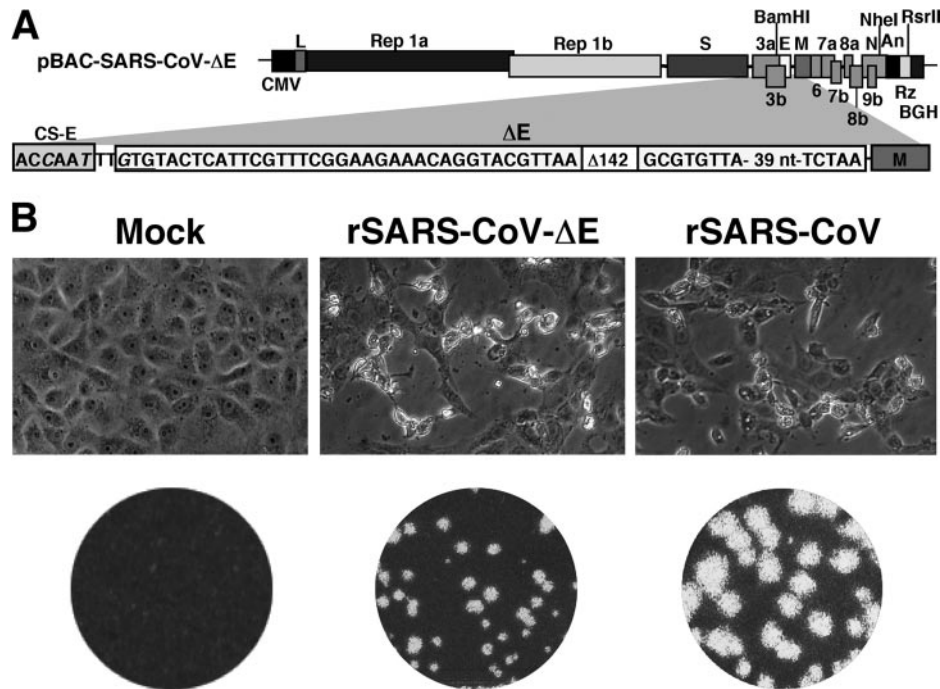


FIG. 1. Rescue of SARS-CoV- Δ E from cDNA in Vero E6 cells. (A) Genetic organization of the rSARS-CoV- Δ E virus. The 142-nt deletion inside the E gene is indicated in a white box (Δ 142). The mutated core sequence (CS-E) within the TRS and the mutated start codon are shown in a box and underlined, respectively. The mutations introduced to change the CS-E and the ATG codon of the E gene are shown in italics. The deleted ORF-E is shown in a box. Restriction sites BamHI, NheI, and RsrII used to delete E gene are indicated. Letters and numbers indicate the viral genes. CMV, cytomegalovirus promoter; L, leader sequence; An, poly(A) tail; Rz, hepatitis delta virus ribozyme; BGH, bovine growth hormone termination and polyadenylation sequences. (B) Cytopathic effect and plaque morphology produced by the indicated viruses on Vero E6 cells.

ment of the cells induced by the rSARS-CoV- Δ E virus was identical to that of the recombinant wild-type virus (Fig. 1B). Nevertheless, smaller plaques were detected with the rSARS-CoV- Δ E virus than with the recombinant wild-type virus (Fig. 1B). The virus was amplified, cloned by three rounds of plaque isolation, and passaged twice to generate a virus stock. At the end of all of these steps, which involve eight passages in tissue culture, no sequence differences related to the emergence of revertants were detected.

The rSARS-CoV- Δ E virus was characterized by immunofluorescence, RT-PCR, and Western blotting. Vero E6 cells were infected with the rSARS-CoV- Δ E or recombinant wild-type virus, and at 20 h postinfection, cells were fixed and analyzed by immunofluorescence microscopy with convalescent-phase serum obtained from a SARS patient (Fig. 2A). The pattern of immunofluorescence was similar for the two viruses and, in both cases, cell membrane and cytoplasmic vesicles were prominently stained.

The synthesis of sgmRNAs was characterized by RT-PCR (Fig. 2B). To amplify viral mRNAs, a forward primer complementary to the leader sequence and reverse primers specific for the S, E, and N genes of SARS-CoV were used. As expected, the 250-bp PCR product from the E gene sgmRNA was not detected in rSARS-CoV- Δ E-infected cells. In addition, PCR products of 1,050 bp in the case of the rSARS-CoV- Δ E virus and of 1,200 bp in the case of the recombinant wild-type virus were identified. The sequence of these PCR products matched that of the sgmRNAs starting at the TRS of gene 3

and confirmed that the rSARS-CoV- Δ E virus maintained the mutations and deletion introduced to prevent E gene expression. In contrast, no differences in the PCR products derived from the mRNA encoding S and N proteins were detected (Fig. 2B).

To analyze whether the deletion of the E protein gene alters the ratios of viral sgmRNAs, the expression of all viral genes was analyzed by quantitative RT-PCR. To amplify viral sgmRNAs, two primers specific for each mRNA were used, one hybridized in the leader sequence, and the other in the coding sequence of each gene (Table 1). The amount of the sgmRNAs was normalized to the genomic RNA. No changes at all, or changes within twofold, which were considered nonsignificant, were detected between the relative amounts of homologous sgmRNA in rSARS-CoV- and rSARS-CoV- Δ E-infected cells (data not shown), suggesting that the deletion of gene E has little influence in the expression of the other sgmRNAs.

The absence of the E protein was also demonstrated by Western blot analysis. Protein extracts of Vero E6 cells infected with the rSARS-CoV- Δ E virus contained S and N proteins but no E protein. Western blot analysis using antibodies against S and N proteins revealed a 170-kDa band and a double band of approximately 46 kDa, respectively. In contrast, Western blot analysis using a specific E protein antibody failed to detect a band of approximately 10 kDa, corresponding to E protein that was observed in the case of rSARS-CoV-infected Vero E6 cell extracts (Fig. 2C). Collectively, these

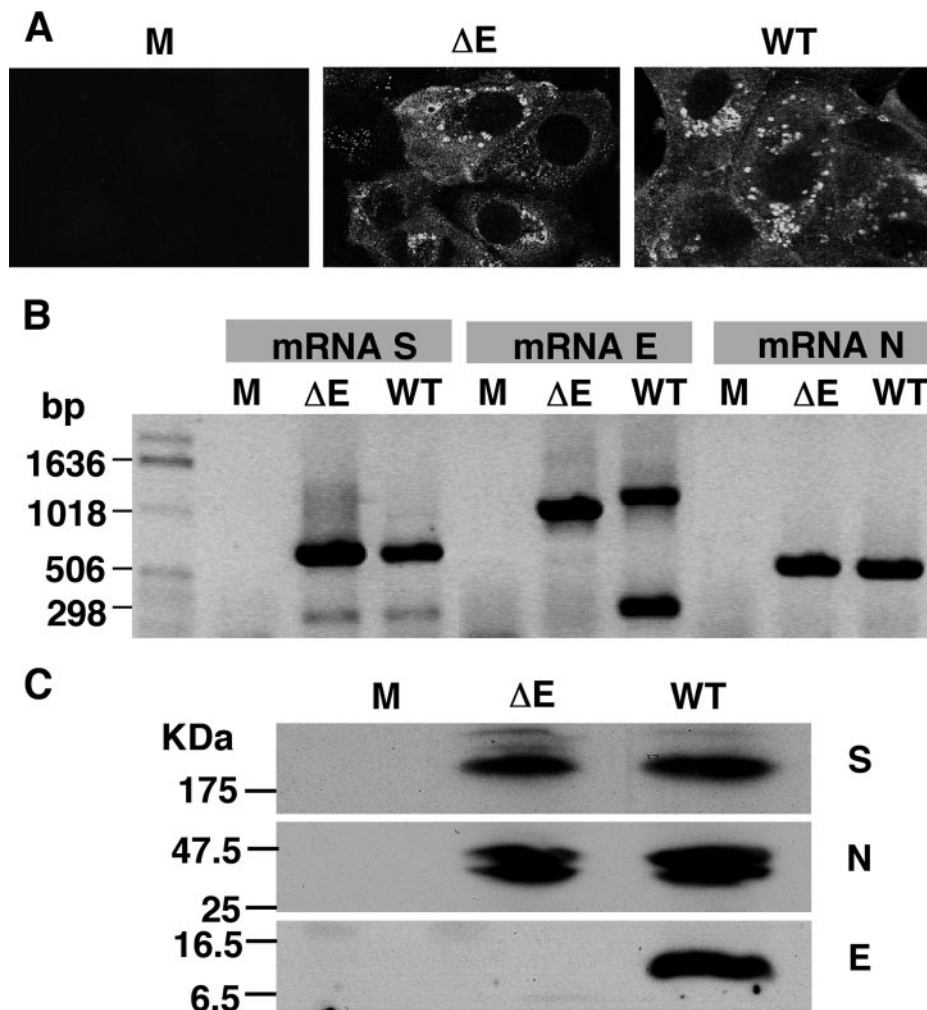


FIG. 2. Characterization of defective virus proteins and mRNAs. Vero E6 cells were mock infected (M) or infected with the rSARS-CoV-ΔE (ΔE) or the recombinant wild-type (WT) viruses. (A) Viral protein expression was analyzed by indirect immunofluorescence 24 h postinfection using a SARS-CoV-specific human polyclonal antibody followed by Cy5-labeled goat anti-human antibody. (B) Viral mRNA expression was analyzed by RT-PCR using the oligonucleotides specific for sgRNAs of S, E, and N genes. (C) Western blot analysis of infected cell lysates using S, N, and E protein-specific polyclonal antibodies followed by peroxidase-labeled goat anti-rabbit antibody.

data indicate that the rSARS-CoV-ΔE has the predicted genome structure and gene expression patterns.

To test whether the phenotypic differences between the rSARS-CoV-ΔE and the recombinant wild-type virus were due solely to the E gene deletion and not to unknown changes introduced inadvertently during the engineering of the cDNA, a wild-type virus was reconstituted by replacing the mutated E gene with the wild-type E gene in the pBAC-SARS-CoV-ΔE construct. As expected, the rescued virus was identical to the wild-type virus in terms of plaque morphology, growth kinetics, and mRNA and protein patterns (data not shown). These results strongly suggested that the behavior of the rSARS-CoV-ΔE mutant was due to the deletion of the E gene and not to any accompanying undesired mutations located elsewhere in the genome.

Growth kinetics of rSARS-CoV-ΔE. Growth kinetics in Vero E6 cells of the rSARS-CoV-ΔE and recombinant wild-type viruses showed similar profiles (Fig. 3A). Cytopathic effect in Vero E6 cells was detected at 24 h postinfection. No delay in

cytopathic effect was detected in rSARS-CoV-ΔE-infected cells. In contrast, in Huh-7 and CaCo-2 cells, cytopathic effect was not detected, even at 72 h postinfection. In Vero E6-infected cells, maximal virus titers were reached between 24 and 48 h postinfection (peak titer was $\sim 10^{6.9}$ PFU/ml for the recombinant wild-type virus). The titer of the rSARS-CoV-ΔE virus was ~ 20 -fold lower than that of the recombinant wild-type virus. In Huh-7 cells, maximal titers were reached 48 h postinfection ($\sim 10^{5.7}$ PFU/ml for the recombinant wild-type virus) (Fig. 3B), whereas in CaCo-2 cells, maximal titers were reached ~ 72 h postinfection ($\sim 10^{5.6}$ PFU/ml for the recombinant wild-type virus) (Fig. 3C). In both Huh-7 and CaCo-2 cell lines, rSARS-CoV-ΔE virus grew to titers ~ 200 -fold lower than that of the recombinant wild-type virus. Although the virus titers obtained in CaCo-2 cells are relatively low, they increased at least 10-fold over those obtained at earlier times. The time postinfection at which 50% of maximal viral production is reached was very similar for the wild-type and defective viruses, irrespective of the cell line used, suggesting that there

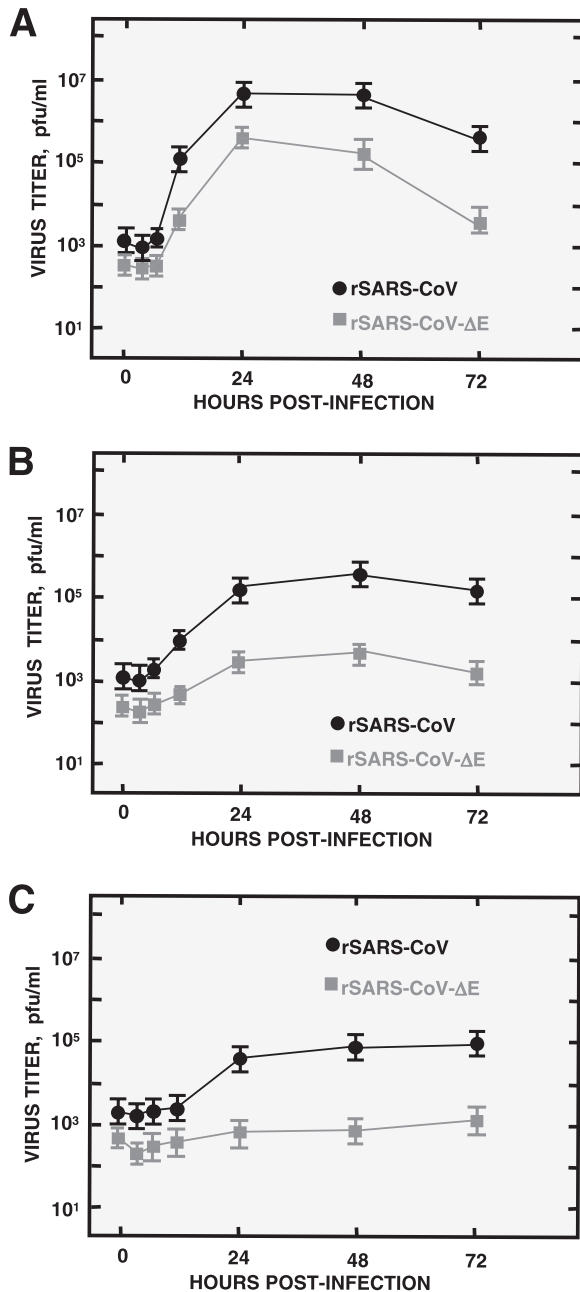


FIG. 3. Growth kinetics of rSARS-CoV- Δ E in different cell lines. Vero E6 (A), Huh-7 (B), and CaCo-2 (C) cells were infected at a MOI of 0.5 with either the rSARS-CoV- Δ E or the recombinant wild-type virus. At different times postinfection, virus titers were determined by plaque assay on Vero E6 cells. Error bars represent standard deviations of the mean of results from three experiments.

was no lag in the release of the defective viruses. These data indicate that although the E protein has a significant effect on SARS-CoV growth, it is not essential for SARS-CoV replication in cell culture.

Stability of rSARS-CoV- Δ E. To analyze whether the E protein influences the stability of SARS-CoV, the effect of temperature and pH on virus infectivity was analyzed. To this end, the recombinant wild-type and rSARS-CoV- Δ E viruses were

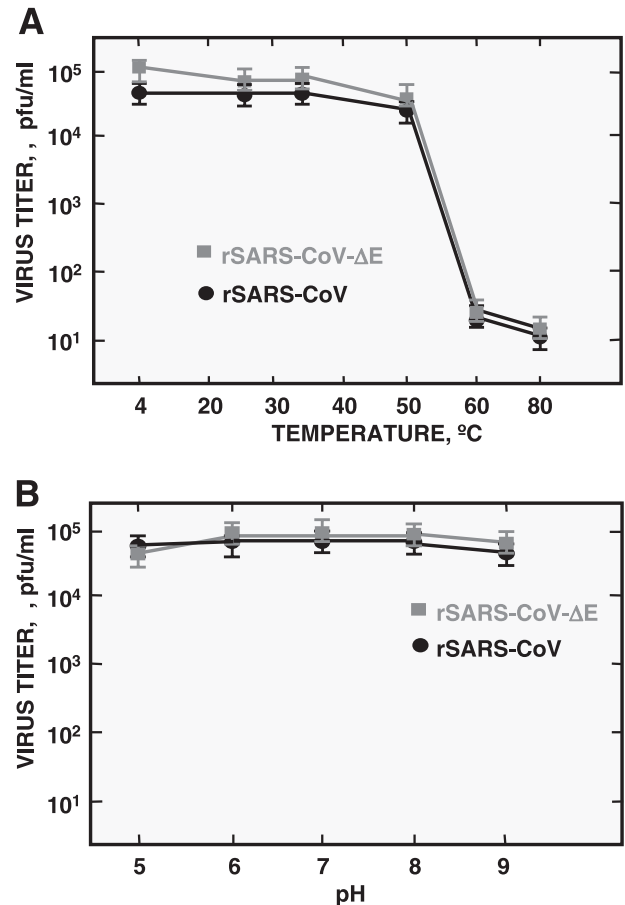


FIG. 4. Effect of temperature and pH changes on rSARS-CoV- Δ E virus infectivity. Supernatants containing recombinant SARS-CoV and SARS-CoV- Δ E viruses were incubated for 30 min at the indicated temperature (A) or pH (B), and virus infectivity was evaluated by titration of culture supernatants on Vero E6 cells. Error bars represent standard deviations of the mean from three experiments. The lower limit of detection is 20 PFU/ml.

incubated at temperatures ranging from 4°C to 80°C for 30 min. Both viruses showed similar inactivation profiles, with a reduction of 10^3 -fold after incubation at 60°C. Heating at 80°C or higher temperatures led to no residual virus infectivity (<20 PFU/ml) (Fig. 4A). Incubation of recombinant wild-type and rSARS-CoV- Δ E viruses at different pHs for 30 min showed that both viruses were stable from pH 5 to 9 (Fig. 4B). These results indicate that the E protein has little influence on the stability of the virions under the different temperatures and pHs tested.

Assembly of rSARS-CoV- Δ E. E protein has been implicated in virus morphogenesis (14, 30). Therefore, the assembly of rSARS-CoV and rSARS-CoV- Δ E viruses was studied by electron microscopy (Fig. 5). The number of the intracellular mature virions present in the cytoplasm was lower in cells infected with rSARS-CoV- Δ E than with the recombinant wild-type virus (Fig. 5A). This observation is consistent with the lower virus titer reached by the defective virus. Coronaviruses assemble by budding into the lumen of Golgi complexes (38). Accordingly, the sites of nucleocapsid invagination into the lumen of the Golgi complexes were analyzed. The number of mature

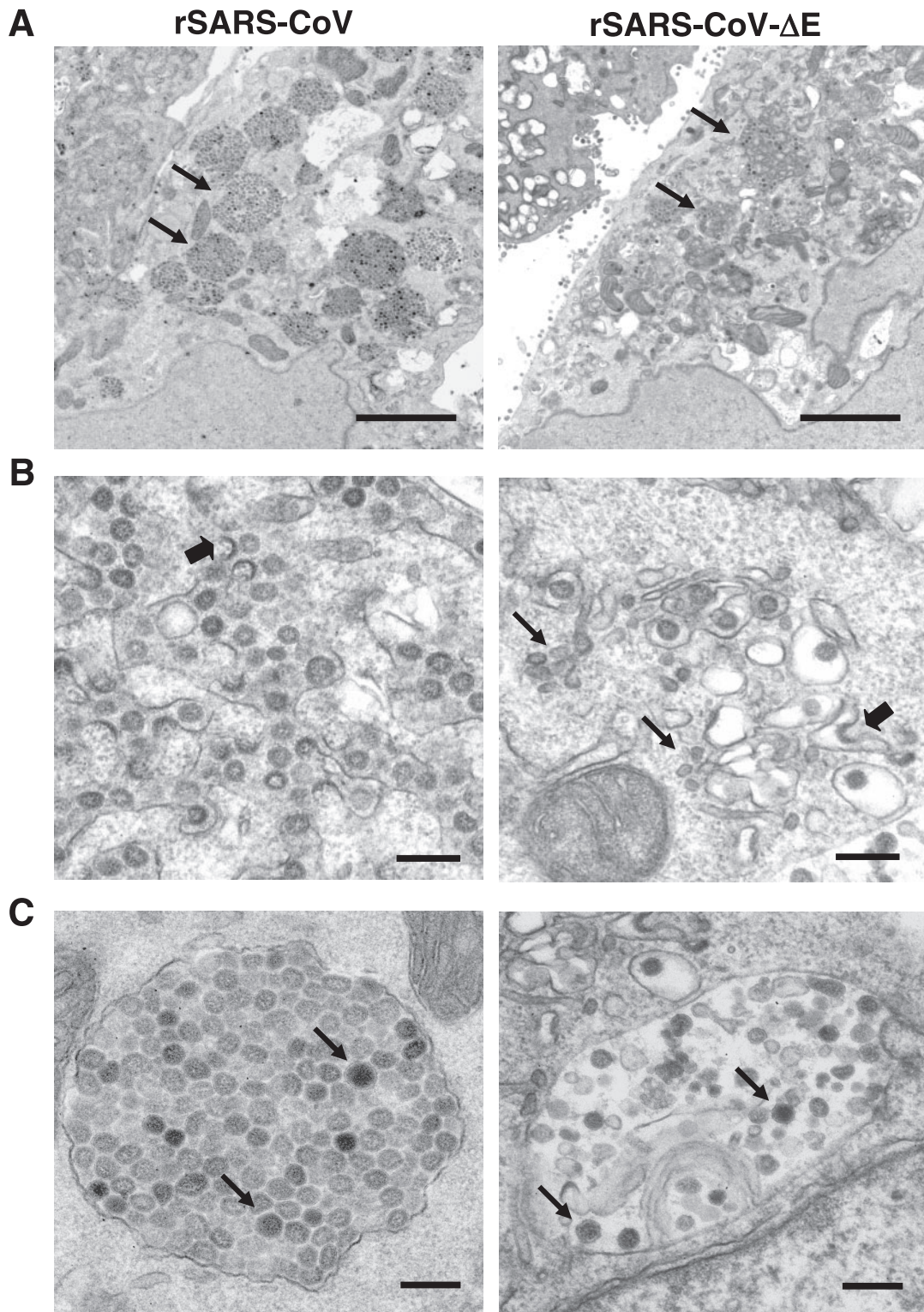


FIG. 5. Ultrastructural analysis of rSARS-CoV- Δ E-infected Vero E6 cells. Vero E6 cells were infected at a MOI of 1 with rSARS-CoV and rSARS-CoV- Δ E viruses, and at 24 h postinfection, the cells were processed for electron microscopy of ultrathin sections. (A) Cytoplasm of an infected cell filled with swollen Golgi sacs containing virus particles (dark arrows). (B) Cytoplasm of infected cells showing the sites of budding of the nucleocapsid into the lumen of swollen Golgi sacs (thick dark arrows). Dense material in the cytoplasm of SARS-CoV- Δ E-infected cells is indicated with dark arrows. (C) Mature virus particles found in swollen Golgi sacs that appeared as large vacuoles (dark arrows). Pictures representing rSARS-CoV-infected cells or rSARS-CoV- Δ E-infected cells are displayed on the left and right sides, respectively. Bars, 2 μ m (A) and 200 nm (B and C).

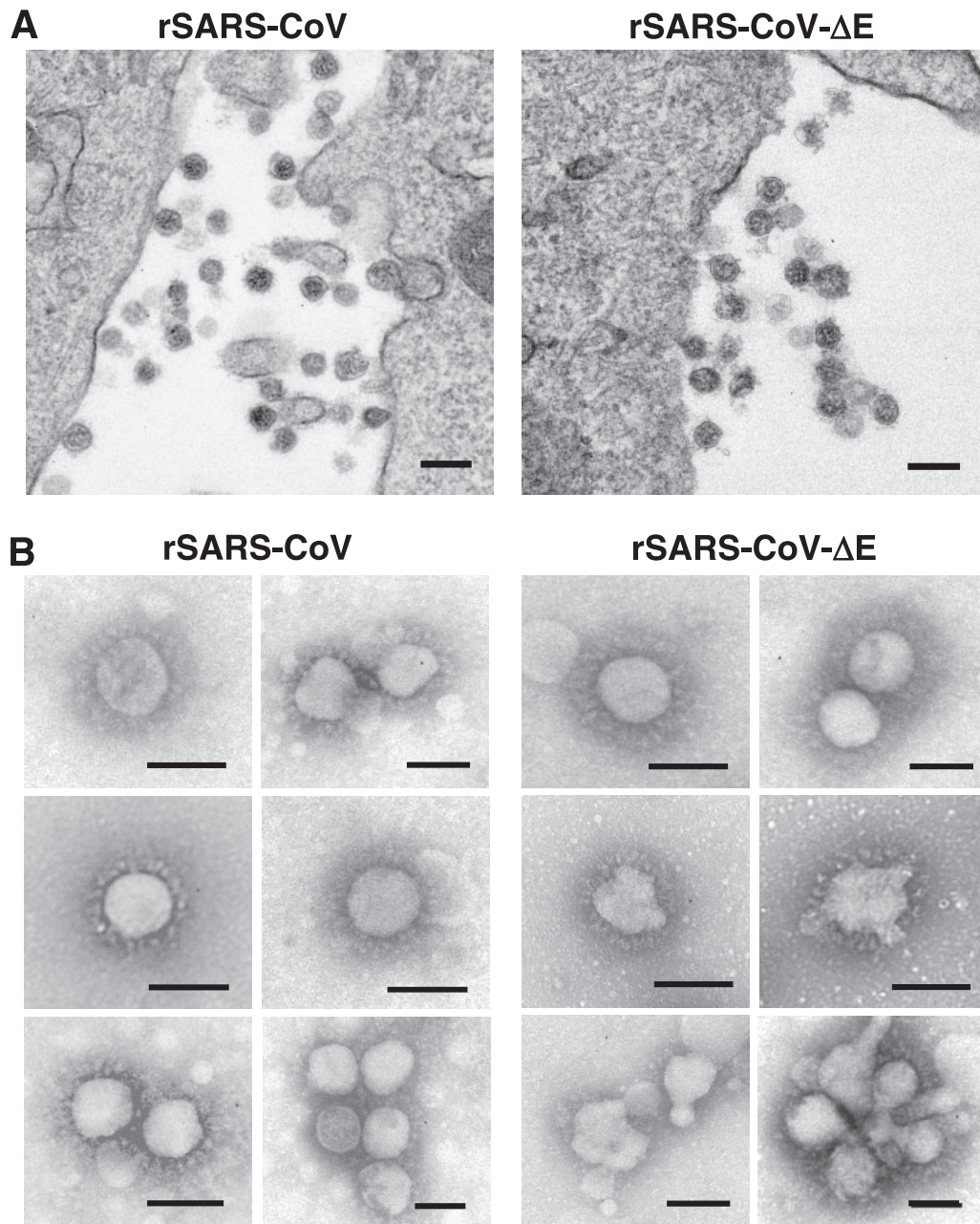


FIG. 6. Morphology of rSARS-CoV-ΔE virions released from infected Vero E6 cells. (A) Electron micrographs of ultrathin sections showing extracellular viruses lining the cell surface. (B) Supernatants of rSARS-CoV- and rSARS-CoV-ΔE-infected cells were concentrated in an airfuge and analyzed by electron microscopy following negative staining with sodium phosphotungstate. Pictures on the left represent rSARS-CoV-infected cells, while those on the right represent rSARS-CoV-ΔE-infected cells. Bars, 200 nm (A) and 100 nm (B).

virions in these sites was lower in the case of rSARS-CoV-ΔE-infected cells than in the recombinant wild-type virus-infected cells, and an increase of dense material in the cytoplasm of rSARS-CoV-ΔE virus-infected cells was observed, probably corresponding to aberrant virions (Fig. 5B). Virus particles were seen in vesicles either as single particles (data not shown) or as groups of viruses in enlarged vesicles (Fig. 5C). In this case, the number of mature virions was considerably higher in the rSARS-CoV-infected cells than in rSARS-CoV-ΔE-infected cells. In addition, vesicles observed in rSARS-CoV-ΔE-

infected cells contained dense, granular material interspersed between the virions that could correspond to aborted viral assembly processes. Overall, these data suggest that the E protein has an important role in assembly.

SARS-CoV virion morphology. The potential influence of E protein deletion on virion morphology was studied by electron microscopic evaluation of ultrathin sections of infected cells and concentrated negative-stained viruses. The extracellular virion morphology observed in ultrathin sections by electron microscopy was similar for rSARS-CoV-ΔE and recombinant

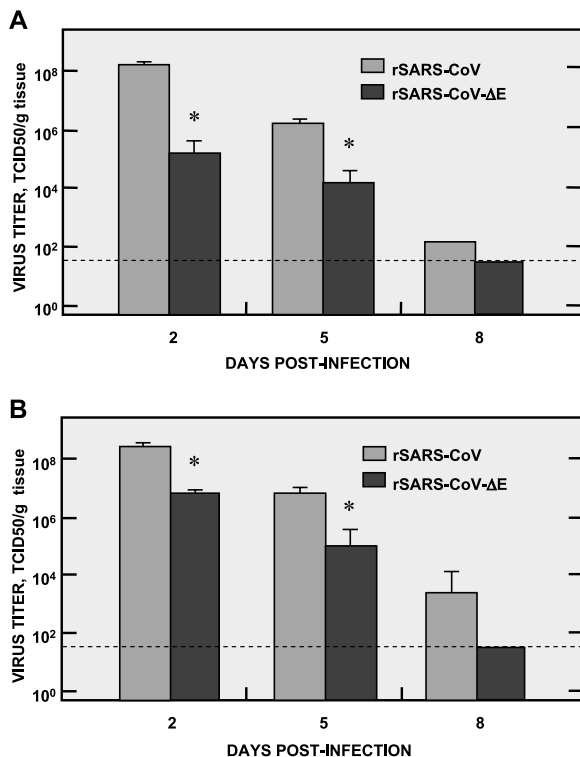


FIG. 7. In vivo growth kinetics of the defective virus. Hamsters were inoculated with 10^3 TCID₅₀ of rSARS-CoV or rSARS-CoV-ΔE. Animals were sacrificed, and tissues were harvested at different times postinfection. Viral titers in the lungs (A) and nasal turbinates (B) were determined in Vero E6 cell monolayers. The nonparametric Mann-Whitney U statistical method was used for ascertaining the significance of observed differences. Statistical significance was indicated by asterisks (P value < 0.05). The dotted line indicates the lower limit of detection.

wild-type viruses, and abnormal structures, such as ellipsoid or tubular forms, were not seen (Fig. 6A).

Negative staining of purified recombinant wild-type and rSARS-CoV-ΔE viruses showed particles surrounded by club-shaped projections, indicating that E protein expression apparently has little influence on virion morphology (Fig. 6B). Nevertheless, purified rSARS-CoV-ΔE virus showed a higher frequency of virus aggregation and amorphous structures than wild-type virus (Fig. 6B). Examination of more than 300 rSARS-CoV and rSARS-CoV-ΔE virions showed that about 10 and 50% of the virions had an amorphous structure in the parental and deletion mutant viruses, respectively. In addition, 20% of the defective virions appeared aggregated, whereas virus association was minimal in the wild-type virus. These data suggest that the defective virus was more sensitive to mechanical shearing forces.

Replication of rSARS-CoV-ΔE in the respiratory tract of hamsters. The in vivo growth of rSARS-CoV and rSARS-CoV-ΔE viruses was determined by infecting Golden Syrian hamsters (44). The animals were sacrificed at 2, 5, and 8 days postinfection. Virus titers in lungs (Fig. 7A) and nasal turbinates (Fig. 7B) of hamsters infected with the rSARS-CoV-ΔE virus were between 100- and 1,000-fold lower than those of the recombinant wild-type virus, suggesting that the rSARS-

CoV-ΔE virus was attenuated in growth in hamsters. Infectious virus was detected in lung and nasal turbinates of animals infected with the recombinant wild-type virus at 8 days postinfection, whereas the defective virus, present at 2 days postinfection, was already cleared at this time point (Fig. 7A).

Pulmonary pathology associated with the replication of the recombinant wild-type and rSARS-CoV-ΔE viruses was compared in Golden Syrian hamsters (43, 44). Animals were sacrificed 2 and 5 days after rSARS-CoV or rSARS-CoV-ΔE infection, and lungs were examined histologically. Pathology was similar at 2 and 5 days postinfection, although it showed higher intensity at 2 days, as it could be expected from the higher virus titers observed at earlier times. Animals infected with the recombinant wild-type virus showed more intense peribronchiolar and interstitial inflammatory infiltrates than those infected with the rSARS-CoV-ΔE virus (Fig. 8A and B). In agreement with the virus titer, the immunohistochemistry analysis revealed a higher antigen concentration in the lungs of rSARS-CoV-infected animals than in rSARS-CoV-ΔE-infected animals (Fig. 8C and D). This indicates that the rSARS-CoV-ΔE virus is attenuated in growth and accompanying pathology in the hamster model.

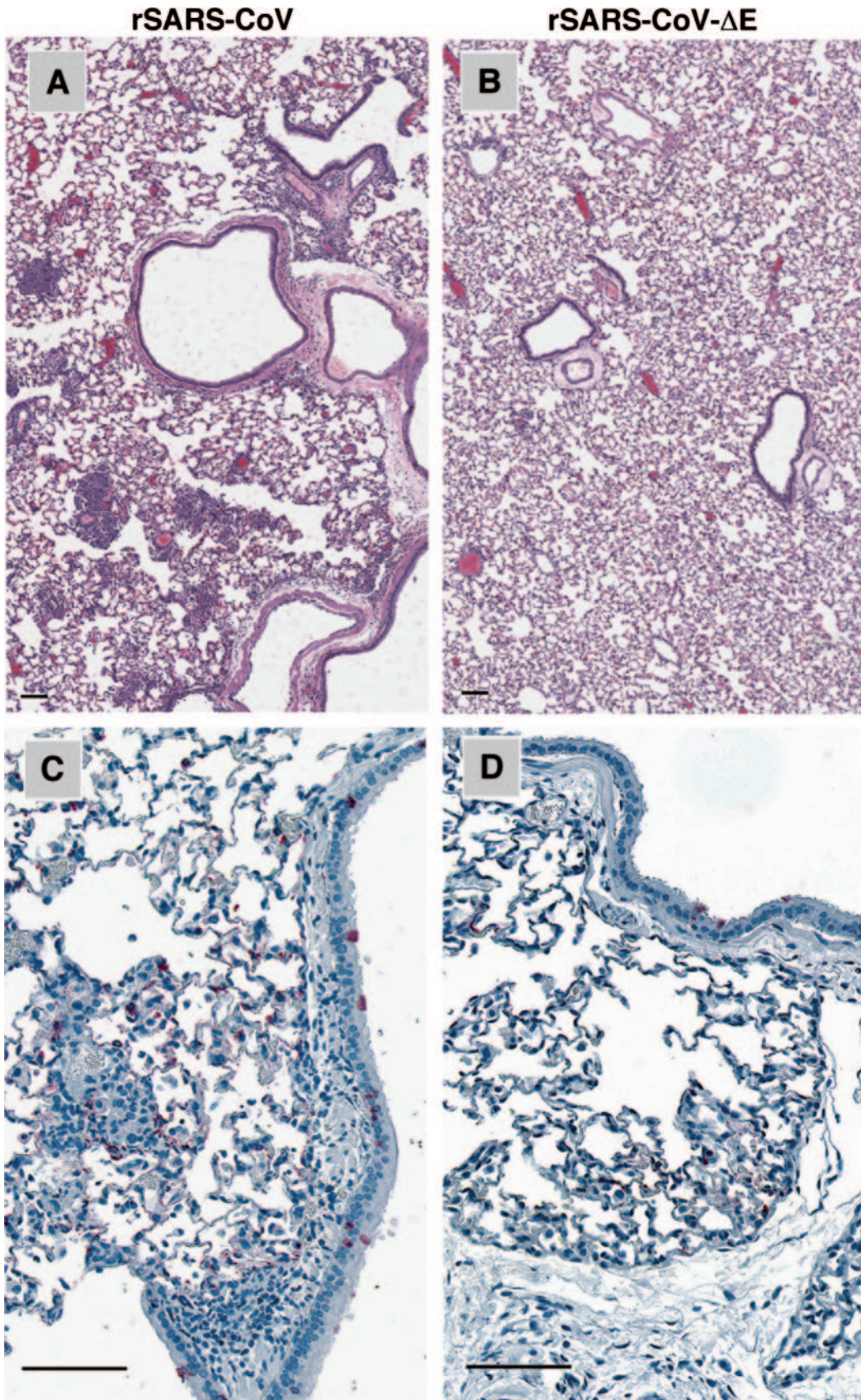
DISCUSSION

A recombinant SARS-CoV that lacks the E gene was engineered using a BAC. The rescued virus was attenuated in vitro and in the hamster model. The E gene was previously shown to be a nonessential gene for the group 2 MHV coronavirus (30), although elimination of this gene reduced virus growth in cell culture more than 1,000-fold. In contrast, for the group 1 TGEV coronavirus, expression of the E gene product was essential for virus release and spread. Release and spread of the TGEV-ΔE virus was restored by providing E protein in *trans* (9, 39), leading to the generation of efficient replication-competent, propagation-deficient virus vectors.

To abolish E gene expression and examine the role of E protein in SARS-CoV propagation, a plasmid encoding a SARS-CoV with a deleted E gene was generated. Interestingly, viable viruses were recovered in Vero E6 cells with a relatively high titer ($>10^5$ PFU/ml), indicating that rSARS-CoV E protein is not essential for virus replication in cell culture. In this respect, SARS-CoV behaves as MHV, the other group 2 coronavirus studied, although rSARS-CoV-ΔE grows to a considerably higher titer. The differential behavior of ΔE mutant viruses from different coronavirus groups may indicate basic differences in virion assembly or life cycles among the different groups.

E proteins from different coronavirus groups have divergent channel selectivity. HCoV-229E group 1 coronavirus E protein shows a preference for K^+ ions, whereas the group 2 MHV and SARS-CoV E proteins, as well as the group 3 coronavirus, IBV E protein, have a greater preference for Na^+ ions (55). Furthermore, it has been shown that E proteins from group 2, bovine coronavirus, and SARS-CoV, as well as the group 3 IBV E protein, can substitute for the E protein of MHV and enhance replication of recombinant MHV. In contrast, the group 1 TGEV protein could not substitute for the MHV E protein in recombinant viruses (35a).

The requirement of E protein in the formation of coronavi-



rus VLPs has also been studied. While it is generally believed that the E protein is required for coronavirus VLP formation, there is disagreement on whether this protein is required for SARS-CoV pseudoparticle assembly. A group of reports describe the requirement of E and M proteins for the efficient assembly of pseudoparticles in insect cells (21, 36), while another report indicates that the N and M proteins are necessary and sufficient for the formation of VLPs in mammalian cells (23). Our results suggest that SARS-CoV E protein is not essential for VLP formation in Vero E6, Huh-7, and CaCo-2 cells, but its presence may considerably increase the efficiency of VLP production. This would be consistent with the observation that TGEV particles are formed in the absence of E protein, although these VLPs did not fully mature and were not released from the cells (J. Ortego, J. E. Ceriani, J. Planadurán, and L. Enjuanes, submitted for publication). Nevertheless, the proteins required for efficient VLP formation could depend on the cell line utilized. We cannot exclude at this time whether factors other than those involved in assembly can contribute to reduced titers in one cell line compared to another.

The titers of rSARS-CoV-ΔE in Vero E6, Huh-7, and CaCo-2 cells were lower than those of the recombinant wild-type virus. No significant differences in inactivation were observed between the recombinant wild-type and rSARS-CoV-ΔE viruses treated at different temperatures and pHs, suggesting that the differences observed in the growth kinetics were due to limitations other than altered virus stability. In agreement with previous reports on SARS-CoV stability, both the recombinant wild-type and rSARS-CoV-ΔE viruses were stable at pHs ranging from 5 to 9 (10). SARS-CoV seems to be more stable than TGEV at different pHs, as it has been reported that incubating TGEV to pH 5 and 9 leads to a decrease in virus titer of at least 200-fold (39).

Electron microscopy of infected cells showed that the production of rSARS-CoV-ΔE was lower than that of the recombinant wild-type virus and that the proportion of dense granular material was higher in the rSARS-CoV-ΔE-infected cells than in rSARS-CoV-infected cells. This dense material might correspond to aberrant assembly processes leading to immature virions, as could be expected if E protein is implicated as a structural component or as a protein that plays a role in virus assembly and budding. The role of E protein in assembly, as a scaffold protein, and budding could be postulated based on the abundance of the protein in infected cells and the low copy number (~20 copies per virion) of this protein in mature virus particles (17, 30, 34, 42). This observation has also been made for the M2 protein of influenza virus, a viral protein functioning as an ion channel that has been implicated in viral assembly (58). Additional studies are needed to determine the specific

steps that are affected during SARS-CoV assembly and morphogenesis in the absence of E protein.

Previous studies have shown that MHV E protein mutants have aberrant morphology (14). In these viruses, clustered charged amino acid-to-alanine mutations were introduced into the E protein. Assuming that charged amino acid residues are more likely located on the protein surface and that these domains often contribute to protein-protein interactions, substitutions of these charged residues with alanine would likely disrupt critical interactions or functions of the mutant E proteins. One proposed role of the E protein is to pinch off the neck of the nascent virion in the budding process. In fact, the SARS-CoV E protein contains a helical hairpin that deforms lipid bilayers by increasing their curvature, providing a molecular role for E protein in viral budding and final virion morphology (2, 26). Nevertheless, our findings would be at variance with such a role as essential for the SARS-CoV E protein since rSARS-CoV-ΔE showed similar morphology as the recombinant wild-type virus, with spherical symmetry and without ellipsoidal or tubular virion forms. This suggests that the E protein has limited or no impact on the apparent morphology of SARS-CoV released from Vero E6 cells. Nevertheless, it seems prudent at this time not to overinterpret these findings because there may be factors that complement the role of the E protein in virus morphogenesis and final virion structure in progeny virions from rSARS-CoV-ΔE-infected Vero E6 cells.

The effect of the deletion of group-specific genes in different coronaviruses has been studied previously. Reports using MHV as a model have shown that deletion of ORFs 4, 5a, 2a, and HE are attenuating in the natural host (12). Similarly, studies deleting ORF 7 of TGEV (40) and ORFs 3abc and 7ab of feline infectious peritonitis virus (19) led to virus attenuation. However, SARS-CoV deletion mutants lacking ORFs 3a, 3b, 6, 7a, and 7b did not significantly influence *in vitro* and *in vivo* replication efficiency in the mouse model (57). A significant difference of our work is that we have deleted a structural protein (E) and that, in this study, the hamster model is used to evaluate rSARS-CoV-ΔE virus pathogenicity because it demonstrates similar features present in human cases of SARS-CoV infections, including interstitial pneumonitis and alveolar damage. Although an ideal animal model that completely reproduces human clinical disease and pathological findings has not been identified, the hamster model reproducibly supports SARS-CoV replication in the respiratory tract to a higher titer and for a longer duration than in mice or non-human primates. Virus replication in this model is accompanied by histologic evidence of pneumonitis, and the animals develop viremia and extrapulmonary spread of virus (43, 44). Although overt clinical disease is absent, the hamster model is an excellent model for the evaluation of SARS-CoV infection.

FIG. 8. Lung pathology caused by rSARS-CoV and rSARS-CoV-ΔE infection in hamsters. Hamsters were inoculated with 10^3 TCID₅₀ of rSARS-CoV or rSARS-CoV-ΔE. Animals were sacrificed 2 days after infection, and lungs were inflated with and fixed in 10% formalin and processed for histopathological examination and immunohistochemistry. (A) Hematoxylin and eosin staining of a lung section shows prominent mononuclear inflammatory infiltrates in peribronchiolar, interstitial, and alveolar spaces. (B) Hematoxylin and eosin staining of a lung section shows scant mononuclear inflammatory infiltrates. (C) Immunoalkaline phosphatase staining shows abundant viral antigens in bronchiolar epithelial cells and alveolar pneumocytes. (D) Scattered immunohistochemical staining of viral antigens in bronchiolar epithelial cells and alveolar pneumocytes. Panels A and C show lung tissues from rSARS-CoV-infected animals. Panels B and D show lung tissues from rSARS-CoV-ΔE-infected animals. Bar, 100 μm.

Titers of rSARS-CoV achieved in the respiratory tract of hamsters were similar to those previously reported (44) and were 100- to 1,000-fold higher than titers of the rSARS-CoV-ΔE virus, suggesting that this mutant virus is attenuated. In humans, the viral load and the duration of viral replication influence disease outcomes (5, 24). Histopathology examination of lungs from infected hamsters was performed at 2 and 5 days postinfection because it has been shown that pulmonary disease was most notable at these time points. In fact, the amounts of pulmonary inflammation and viral antigen were both less in lungs from rSARS-CoV-ΔE-infected hamsters than in rSARS-CoV-infected animals, indicating that rSARS-CoV-ΔE is attenuated in vivo.

To our knowledge, this is the first study describing an engineered, mutant SARS-CoV that is attenuated in vivo. A reduction of SARS-CoV titers in patients has been associated with a considerable reduction in pathogenicity and an increase in survival rates (5, 24). This attenuated virus will be of interest to the scientific community as a research tool because of a reduction in risk associated with its use in laboratory studies. Although there are aspects of the biology of the virus that will require confirmation with wild-type SARS-CoV strains, rSARS-CoV-ΔE mutants pseudotyped with S genes from antigenically diverse strains could be useful tools to study virus neutralization and vaccine efficacy under safer conditions than those in which fully infectious SARS-CoV pseudotypes are being used.

ACKNOWLEDGMENTS

We thank P. Pérez-Breña from the Human Health Department (Instituto de Salud Carlos III, Madrid, Spain) for facilitating the development of the project, D. Dorado and M. González for technical assistance, Jadon Jackson for valuable assistance in the animal studies, and C. Galán for collaboration with the quantitative RT-PCR experiments.

This work was supported by grants from the Ministry of Education and Science of Spain (BIO2004-00636), the European Community (Frame VI, DISSECT PROJECT, SP22-CT-2004-511060), and Fort Dodge Veterinaria. M.L.D. received a fellowship from the Ministry of Education and Science of Spain. This research was supported in part by the Intramural Research Program of the NIH, NIAID.

REFERENCES

- Almazán, F., M. L. DeDiego, C. Galan, D. Escors, E. Alvarez, J. Ortego, I. Sola, S. Zúñiga, S. Alonso, J. L. Moreno, A. Nogales, C. Capiscol, and L. Enjuanes. 2006. Construction of a SARS-CoV infectious cDNA clone and a replicon to study coronavirus RNA synthesis. *J. Virol.* **80**:10900–10906.
- Arbely, E., Z. Khattari, G. Brotons, M. Akkawi, T. Salditt, and I. T. Arkin. 2004. A highly unusual palindromic transmembrane helical hairpin formed by SARS coronavirus E protein. *J. Mol. Biol.* **341**:769–779.
- Baudoux, P., C. Carrat, L. Besnardeau, B. Charley, and H. Laude. 1998. Coronavirus pseudoparticles formed with recombinant M and E proteins induce alpha interferon synthesis by leukocytes. *J. Virol.* **72**:8636–8643.
- Brierley, I., P. Digard, and S. C. Inglis. 1989. Characterization of an efficient coronavirus ribosomal frameshifting signal: requirement for an RNA pseudoknot. *Cell* **57**:537–547.
- Chu, C. M., L. L. Poon, V. C. Cheng, K. S. Chan, I. F. Hung, M. M. Wong, K. H. Chan, W. S. Leung, B. S. Tang, V. L. Chan, W. L. Ng, T. C. Sim, P. W. Ng, K. I. Law, D. M. Tse, J. S. Peiris, and K. Y. Yuen. 2004. Initial viral load and the outcomes of SARS. *Can. Med. Assoc. J.* **171**:1349–1352.
- Corse, E., and C. E. Machamer. 2002. The cytoplasmic tail of infectious bronchitis virus E protein directs Golgi targeting. *J. Virol.* **76**:1273–1284.
- Corse, E., and C. E. Machamer. 2003. The cytoplasmic tails of infectious bronchitis virus E and M proteins mediate their interaction. *Virology* **312**:25–34.
- Corse, E., and C. E. Machamer. 2000. Infectious bronchitis virus E protein is targeted to the Golgi complex and directs release of virus-like particles. *J. Virol.* **74**:4319–4326.
- Curtis, K. M., B. Yount, and R. S. Baric. 2002. Heterologous gene expression from transmissible gastroenteritis virus replicon particles. *J. Virol.* **76**:1422–1434.
- Darnell, M. E., K. Subbarao, S. M. Feinstone, and D. R. Taylor. 2004. Inactivation of the coronavirus that induces severe acute respiratory syndrome, SARS-CoV. *J. Virol. Methods* **121**:85–91.
- de Haan, C. A. M., L. Kuo, P. S. Masters, H. Vennema, and P. J. M. Rottier. 1998. Coronavirus particle assembly: primary structure requirements of the membrane protein. *J. Virol.* **72**:6838–6850.
- de Haan, C. A. M., P. S. Masters, S. Shen, S. Weiss, and P. J. M. Rottier. 2002. The group-specific murine coronavirus genes are not essential, but their deletion, by reverse genetics, is attenuating in the natural host. *Virology* **296**:177–189.
- Drosten, C., S. Günther, W. Preiser, S. van der Werf, H.-R. Brodt, S. Becker, H. Rabenau, M. Panning, L. Kolesnikova, R. A. M. Fouchier, A. Berger, A.-M. Burguiere, J. Cinatl, M. Eickmann, N. Escriou, K. Grywna, S. Kramme, J.-C. Manuguerra, S. Muller, W. Rickerts, M. V. Stürmer, S. Vieth, H.-D. Klenk, A. D. M. E. Osterhaus, H. Schmitz, and H. W. Doerr. 2003. Identification of a novel coronavirus in patients with severe acute respiratory syndrome. *N. Engl. J. Med.* **348**:1967–1976.
- Fischer, F., C. F. Stegen, P. S. Masters, and W. A. Samsonoff. 1998. Analysis of constructed E gene mutants of mouse hepatitis virus confirms a pivotal role for E protein in coronavirus assembly. *J. Virol.* **72**:7885–7894.
- Fouchier, R. A., T. Kuiken, M. Schutten, G. van Amerongen, G. J. van Doornum, B. G. van den Hoogen, M. Peiris, W. Lim, K. Stohr, and A. D. Osterhaus. 2003. Aetiology: Koch's postulates fulfilled for SARS virus. *Nature* **423**:240.
- Gillim-Ross, L., J. Taylor, D. R. Scholl, J. Ridenour, P. S. Masters, and D. E. Wentworth. 2004. Discovery of novel human and animal cells infected by the severe acute respiratory syndrome coronavirus by replication-specific multiplex reverse transcription-PCR. *J. Clin. Microbiol.* **42**:3196–3206.
- Godet, M., R. L'Haridon, J. F. Vautherot, and H. Laude. 1992. TGEV coronavirus ORF4 encodes a membrane protein that is incorporated into virions. *Virology* **188**:666–675.
- Gorbalenya, A. E., E. J. Snijder, and W. J. Spaan. 2004. Severe acute respiratory syndrome coronavirus phylogeny: toward consensus. *J. Virol.* **78**:7863–7866.
- Haijema, B. J., H. Volders, and P. J. Rottier. 2004. Live, attenuated coronavirus vaccines through the directed deletion of group-specific genes provide protection against feline infectious peritonitis. *J. Virol.* **78**:3863–3871.
- Hattermann, K., M. A. Muller, A. Nitsche, S. Wendt, O. Donoso Mantke, and M. Niedrig. 2005. Susceptibility of different eukaryotic cell lines to SARS-coronavirus. *Arch. Virol.* **150**:1023–1031.
- Ho, Y., P. H. Lin, C. Y. Liu, S. P. Lee, and Y. C. Chao. 2004. Assembly of human severe acute respiratory syndrome coronavirus-like particles. *Biochem. Biophys. Res. Commun.* **318**:833–838.
- Huang, C., N. Ito, C. T. Tseng, and S. Makino. 2006. Severe acute respiratory syndrome coronavirus 7a accessory protein is a viral structural protein. *J. Virol.* **80**:7287–7294.
- Huang, Y., Z. Y. Yang, W. P. Kong, and G. J. Nabel. 2004. Generation of synthetic severe acute respiratory syndrome coronavirus pseudoparticles: implications for assembly and vaccine production. *J. Virol.* **78**:12557–12565.
- Hung, I. F., V. C. Cheng, A. K. Wu, B. S. Tang, K. H. Chan, C. M. Chu, M. M. Wong, W. T. Hui, L. L. Poon, D. M. Tse, K. S. Chan, P. C. Woo, S. K. Lau, J. S. Peiris, and K. Y. Yuen. 2004. Viral loads in clinical specimens and SARS manifestations. *Emerg. Infect. Dis.* **10**:1550–1557.
- Ito, N., E. C. Mossel, K. Narayanan, V. L. Popov, C. Huang, T. Inoue, C. J. Peters, and S. Makino. 2005. Severe acute respiratory syndrome coronavirus 3a protein is a viral structural protein. *J. Virol.* **79**:3182–3186.
- Khattari, Z., G. Brotons, M. Akkawi, E. Arbely, I. T. Arkin, and T. Salditt. 2006. SARS coronavirus E protein in phospholipid bilayers: an x-ray study. *Biophys. J.* **90**:2038–2050.
- Ksiazek, T. G., D. Erdman, C. Goldsmith, S. Zaki, T. Peret, S. Emery, S. Tong, C. Urbani, J. A. Comer, W. Lim, P. E. Rollin, S. Dowell, A.-E. Ling, C. Humphrey, W.-J. Shieh, J. Guarnier, C. D. Paddock, P. Rota, B. Fields, J. DeRisi, J.-Y. Yang, N. Cox, J. Hughes, J. W. LeDuc, W. J. Bellini, and L. J. Anderson. 2003. A novel coronavirus associated with severe acute respiratory syndrome. *N. Engl. J. Med.* **348**:1953–1966.
- Kuiken, T., R. A. M. Fouchier, M. Schutten, G. F. Rimmelzwaan, G. van Amerongen, D. van Riel, J. D. Laman, T. de Jong, G. van Doornum, W. Lim, A. E. Ling, P. K. S. Chan, J. S. Tam, M. C. Zambon, R. Gopal, C. Drosten, S. van der Werf, N. Escriou, J.-C. Manuguerra, K. Stohr, and J. S. M. Peiris. 2003. Newly discovered coronavirus as the primary cause of severe acute respiratory syndrome. *Lancet* **362**:263–270.
- Reference deleted.
- Kuo, L., and P. S. Masters. 2003. The small envelope protein E is not essential for murine coronavirus replication. *J. Virol.* **77**:4597–4608.
- Liao, Y., J. Lescar, J. P. Tam, and D. X. Liu. 2004. Expression of SARS-coronavirus envelope protein in *Escherichia coli* cells alters membrane permeability. *Biochem. Biophys. Res. Commun.* **325**:374–380.
- Liao, Y., Q. Yuan, J. Torres, J. P. Tam, and D. X. Liu. 2006. Biochemical and functional characterization of the membrane association and membrane

- permeabilizing activity of the severe acute respiratory syndrome coronavirus envelope protein. *Virology* **349**:264–265.
33. Madan, V., J. Garcia Mde, M. A. Sanz, and L. Carrasco. 2005. Viroporin activity of murine hepatitis virus E protein. *FEBS Lett.* **579**:3607–3612.
 34. Maeda, J., J. F. Repass, A. Maeda, and S. Makino. 2001. Membrane topology of coronavirus E protein. *Virology* **281**:163–169.
 35. Marra, M. A., S. J. M. Jones, C. R. Astell, R. A. Holt, A. Brooks-Wilson, Y. S. N. Butterfield, J. Khattri, J. K. Asano, S. A. Barber, S. Y. Chan, A. Cloutier, S. M. Coughlin, D. Freeman, N. Girn, O. L. Griffith, S. R. Leach, M. Mayo, H. McDonald, S. B. Montgomery, P. K. Pandoh, A. S. Petrescu, A. G. Robertson, J. E. Schein, A. Siddiqui, D. E. Smailus, J. M. Stott, G. S. Yang, F. Plummer, A. Andonov, H. Artsob, N. Bastien, K. Bernard, T. F. Booth, D. Bowness, M. Czub, M. Drebot, L. Fernando, R. Flick, M. Garbutt, M. Gray, A. Grolla, S. Jones, H. Feldmann, A. Meyers, A. Kabani, Y. Li, S. Normand, U. Stroher, G. A. Tipples, S. Tyler, R. Vogrig, D. Ward, B. Watson, R. C. Brunham, M. Krajden, M. Petric, D. M. Skowronski, C. Upton, and R. L. Roper. 2003. The genome sequence of the SARS-associated coronavirus. *Science* **300**:1399–1404.
 - 35a. Masters, P. S., L. Kuo, R. Ye, K. R. Hurst, C. A. Koetzner, and B. Hsue. 2006. Genetic and molecular biological analysis of protein-protein interactions in coronavirus assembly. *Adv. Exp. Med. Biol.* **581**:163–173.
 36. Mortola, E., and P. Roy. 2004. Efficient assembly and release of SARS coronavirus-like particles by a heterologous expression system. *FEBS Lett.* **576**:174–178.
 37. Mossel, E. C., C. Huang, K. Narayanan, S. Makino, R. B. Tesh, and C. J. Peters. 2005. Exogenous ACE2 expression allows refractory cell lines to support severe acute respiratory syndrome coronavirus replication. *J. Virol.* **79**:3846–3850.
 38. Ng, M. L., S. H. Tan, E. E. See, E. E. Ooi, and A. E. Ling. 2003. Proliferative growth of SARS coronavirus in Vero E6 cells. *J. Gen. Virol.* **84**:3291–3303.
 39. Ortego, J., D. Escors, H. Laude, and L. Enjuanes. 2002. Generation of a replication-competent, propagation-deficient virus vector based on the transmissible gastroenteritis coronavirus genome. *J. Virol.* **76**:11518–11529.
 40. Ortego, J., I. Sola, F. Almazan, J. E. Ceriani, C. Riquelme, M. Balasch, J. Plana-Durán, and L. Enjuanes. 2003. Transmissible gastroenteritis coronavirus gene 7 is not essential but influences *in vivo* virus replication and virulence. *Virology* **308**:13–22.
 41. Peiris, J. S. M., S. T. Lai, L. L. M. Poon, Y. Guan, L. Y. C. Yam, W. Lim, J. Nicholls, W. K. S. Yee, W. W. Yan, and M. T. Cheung. 2003. Coronavirus as a possible cause of severe acute respiratory syndrome. *Lancet* **361**:1319–1325.
 42. Raamsman, M. J. B., J. K. Locker, A. de Hooge, A. A. F. de Vries, G. Griffiths, H. Vennema, and P. J. M. Rottier. 2000. Characterization of the coronavirus mouse hepatitis virus strain A59 small membrane protein E. *J. Virol.* **74**:2333–2342.
 43. Roberts, A., W. D. Thomas, J. Guarner, E. W. Lamirande, G. J. Babcock, T. C. Greenough, L. Vogel, N. Hayes, J. L. Sullivan, S. Zaki, K. Subbarao, and D. M. Ambrosino. 2006. Therapy with a severe acute respiratory syndrome-associated coronavirus-neutralizing human monoclonal antibody reduces disease severity and viral burden in golden Syrian hamsters. *J. Infect. Dis.* **193**:685–692.
 44. Roberts, A., L. Vogel, J. Guarner, N. Hayes, B. Murphy, S. Zaki, and K. Subbarao. 2005. Severe acute respiratory syndrome coronavirus infection of golden Syrian hamsters. *J. Virol.* **79**:503–511.
 45. Rota, P. A., M. S. Oberste, S. S. Monroe, W. A. Nix, R. Campgiani, J. P. Icenogle, S. Peñaranda, B. Bankamp, K. Maher, M.-H. Chen, S. Tong, A. Tamin, L. Lowe, M. Frace, J. L. DeRisi, Q. Chen, D. Wang, D. D. Erdman, T. C. T. Peret, C. Burns, T. G. Ksiazek, P. E. Rollin, A. Sanchez, S. Liffick, B. Holloway, J. Limor, K. McCaustland, M. Olsen-Rassmussen, R. Fouchier, S. Gunther, A. D. M. E. Osterhaus, C. Drosten, M. A. Pallansch, L. J. Anderson, and W. J. Bellini. 2003. Characterization of a novel coronavirus associated with severe acute respiratory syndrome. *Science* **300**:1394–1399.
 46. Shen, S., P. S. Lin, Y. C. Chao, A. Zhang, X. Yang, S. G. Lim, W. Hong, and Y. J. Tan. 2005. The severe acute respiratory syndrome coronavirus 3a is a novel structural protein. *Biochem. Biophys. Res. Commun.* **330**:286–292.
 47. Siddell, S. G. 1995. The *Coronaviridae*. Plenum Press, New York, NY.
 48. Snijder, E. J., P. J. Bredenbeek, J. C. Dobbe, V. Thiel, J. Ziebuhr, L. L. M. Poon, Y. Guan, M. Rozanov, W. J. M. Spaan, and A. E. Gorbalenya. 2003. Unique and conserved features of genome and proteome of SARS-coronavirus, an early split-off from the coronavirus group 2 lineage. *J. Mol. Biol.* **331**:991–1004.
 49. Subbarao, K., J. McAuliffe, L. Vogel, G. Fahle, S. Fischer, K. Tatti, M. Packard, W. J. Shieh, S. Zaki, and B. Murphy. 2004. Prior infection and passive transfer of neutralizing antibody prevent replication of severe acute respiratory syndrome coronavirus in the respiratory tract of mice. *J. Virol.* **78**:3572–3577.
 50. Thiel, V., K. A. Ivanov, A. Putics, T. Hertzog, B. Schelle, S. Bayer, B. Wessbrich, E. J. Snijder, H. Rabenau, H. W. Doerr, A. E. Gorbalenya, and J. Ziebuhr. 2003. Mechanisms and enzymes involved in SARS coronavirus genome expression. *J. Gen. Virol.* **84**:2305–2315.
 51. Torres, J., K. Parthasarathy, X. Lin, R. Saravanan, and D. X. Liu. 2006. Model of a putative pore: the pentameric {alpha}-helical bundle of SARS coronavirus E protein in lipid bilayers. *Biophys. J.* **91**:938–947.
 52. van der Hoek, L., K. Pyrc, M. F. Jebbink, W. Vermeulen-Oost, R. J. Berkhout, K. C. Wolthers, P. M. Wertheim-van Dillen, J. Kaandorp, J. Spaargaren, and B. Berkhout. 2004. Identification of a new human coronavirus. *Nat. Med.* **10**:368–373.
 53. Vennema, H., G. J. Godeke, J. W. A. Rossen, W. F. Voorhout, M. C. Horzinek, D. J. Opstelten, and P. J. M. Rottier. 1996. Nucleocapsid-independent assembly of coronavirus-like particles by co-expression of viral envelope protein genes. *EMBO J.* **15**:2020–2028.
 54. Weiss, S. R., and S. Navas-Martin. 2005. Coronavirus pathogenesis and the emerging pathogen severe acute respiratory syndrome coronavirus. *Microbiol. Mol. Biol. Rev.* **69**:635–664.
 55. Wilson, L., P. Gage, and G. Ewart. 2006. Hexamethylene amiloride blocks E protein ion channels and inhibits coronavirus replication. *Virology* **353**:294–306.
 56. Wilson, L., C. McKinlay, P. Gage, and G. Ewart. 2004. SARS coronavirus E protein forms cation-selective ion channels. *Virology* **330**:322–331.
 57. Yount, B., R. S. Roberts, A. C. Sims, D. Deming, M. B. Frieman, J. Sparks, M. R. Denison, N. Davis, and R. S. Baric. 2005. Severe acute respiratory syndrome coronavirus group-specific open reading frames encode nonessential functions for replication in cell cultures and mice. *J. Virol.* **79**:14909–14922.
 58. Zebedee, S. L., C. D. Richardson, and R. A. Lamb. 1985. Characterization of the influenza virus M2 integral membrane protein and expression at the infected-cell surface from cloned cDNA. *J. Virol.* **56**:502–511.
 59. Ziebuhr, J., E. J. Snijder, and A. E. Gorbalenya. 2000. Virus-encoded proteinases and proteolytic processing in the *Nidovirales*. *J. Gen. Virol.* **81**:853–879.
 60. Zúñiga, S., I. Sola, S. Alonso, and L. Enjuanes. 2004. Sequence motifs involved in the regulation of discontinuous coronavirus subgenomic RNA synthesis. *J. Virol.* **78**:980–994.